Applied Catalysis A: General 469 (2014) 33–44

Contents lists available at ScienceDirect

Applied Catalysis A: General

journal homepage: www.elsevier.com/locate/apcata

Synthesis of reverse micelle α-FeOOH nanoparticles in ionic liquid as an only electrolyte: Inhibition of electron–hole pair recombination for efficient photoactivity

R. Jusoh[a], A.A. Jalil[a,*], S. Triwahyono[b], A. Idris[c], S. Haron[a], N. Sapawe[a], N.F. Jaafar[b], N.W.C. Jusoh[a]

[a] Institute of Hydrogen Economy, Department of Chemical Engineering, Faculty of Chemical Engineering, Universiti Teknologi Malaysia, 81310 UTM Johor Bahru, Johor, Malaysia
[b] Ibnu Sina Institute for Fundamental Science Studies, Faculty of Science, Universiti Teknologi Malaysia, 81310 UTM Johor Bahru, Johor, Malaysia
[c] Institute of Bioproduct Development, Department of Chemical Engineering, Faculty of Chemical Engineering, Universiti Teknologi Malaysia, 81310 UTM Johor Bahru, Johor, Malaysia

ARTICLE INFO

Article history:
Received 27 April 2013
Received in revised form 30 August 2013
Accepted 28 September 2013
Available online xxx

Keywords:
α-FeOOH nanoparticles
Ionic liquid
Reverse micelle
Photo-Fenton-like
2-Chlorophenol

ABSTRACT

Discrete α-FeOOH nanoparticles (5–10 nm) were synthesized by a simple electrochemical method using an ionic liquid (IL), dodecyltrimethylammonium bromide (IL – FeOOH). IL that acts as an only electrolyte is capable of producing IL – FeOOH nanoparticles without any agglomeration. Its crystallinity, morphology, functional characteristics, and surface area were analyzed using an X-ray diffractometer, a transmission electron microscope, a Fourier-transform infrared spectrometer, and the Brunnauer–Emmett–Teller (BET) method, respectively. The characterization results verified that reverse micelle formation of IL plays an important role in the stabilization and miniaturization of the α-FeOOH nanoparticles. The activity of IL-FeOOH was tested on a photo-Fenton-like degradation of 2-chlorophenol (2-CP). Results showed that a nearly neutral condition of pH 5 was able to completely degrade 2-CP within 180 min of reaction at 50 °C, using 0.03 g L^{-1} of catalyst dosage and 50 mg L^{-1} of 2-CP initial concentration, with only a small amount of H_2O_2 (0.156 mM). It was found that the reverse micelle formed around the catalyst surface could trap the photogenerated electron to inhibit the recombination of photo-induced electron–hole pairs thus enhancing its catalytic activity. Kinetic studies using the Langmuir–Hinshelwood model illustrated that a surface reaction was the controlling step of the process. A reusability study showed that the catalyst was still stable after four subsequent reactions as shown by infrared spectroscopy. The results provide strong evidence to support the potential use of using IL as an alternative electrolyte to synthesize photo-Fenton-like nanocatalyst that can be used to treat organic pollutants such as 2-CP.

1. Introduction

In the huge array of organic pollutants generated by man-made activities, a sizable fraction belongs to various chlorinated phenol compounds. Among them, 2-chlorophenol (2-CP) is used in various chemical processes such as in agriculture, paper, cosmetic, biocide, and public health industries. They belong to the large group of hazardous pollutants presenting serious threats to the surrounding ecosystem [1] and the lethal dosage values (LD_{50}) determined in mice indicate that 2-CP is considerably more toxic than dichlorophenols [2]. When released into the environment, they can cause negative effects to aquatic organisms, while in higher concentrations they present a serious threat to humans as well since chlorinated compounds are known to be the starting material for dioxins and furans [3,4]. Thus, an efficient treatment is required to avoid the environmental impact caused by these harmful and recalcitrant pollutants.

The ability of biological and physical methods in the treatment of chlorophenols can be successfully applied, but demand for secondary treatment should be taken into account as well [5]. Chlorophenols do not undergo direct sunlight photolysis in the natural environment since they only absorb light below 290 nm [2]. Therefore, advanced oxidation technologies (AOTs) present a promising alternative to common treatment methods. AOTs are based on the generation of hydroxyl radicals (•OH), a reactive species capable of degrading or mineralizing the majority of organics [6,7]. The integration of two different AOTs (photocatalytic and Fenton-like) often offers synergistic reaction routes for the production of •OH [8], and has been shown to be suitable for the

* Corresponding author. Tel.: +60 7 5535581, fax: +60 7 5536165.
E-mail address: aishah@cheme.utm.my (A.A. Jalil).

0926-860X/$ – see front matter © 2013 Elsevier B.V. All rights reserved.
http://dx.doi.org/10.1016/j.apcata.2013.09.046

degradation of various chlorinated phenol pollutants [9–11]. The development of this catalytic system, which works not only under UV light but also under visible light, has been a great concern regarding the efficient utilization of solar light and the need to address the world's energy problems [12]. However, the photo-Fenton-like catalysts used generally face a practical problem, i.e., the undesired electron–hole pair recombination that represents a major energy-wasting step that may hinder the system efficiency under visible light irradiation [13]. In addition, in the photo-Fenton-like system, the fastest rates in solution are observed at strong acidic pH [14], which introduces the need for acidification of the reacting medium and subsequent neutralization after treatment. Thus, nearly neutral condition appears more favorable in employing the photo-Fenton-like system, thus encouraging an attempt to conduct the system under mild pH conditions [15]. On the other hand, disproportionate excess concentration of the oxidizing agent (e.g., H_2O_2), which is induced by the high electron–hole recombination rate, can result in negative effects of the photo-Fenton-like system [16]. To overcome this shortcoming, some strategies have been exploited to decrease electron–hole recombination efficiency, including metal or non-metal elements doping, surface modification, coupling with other semiconductors, and inclusion of electron acceptors [17–20]. Some authors have conducted their work with high H_2O_2 concentration (20.0 mM) and others have used ~2.0 mM H_2O_2 [14,21–25]. Since the selection of a reduced H_2O_2 concentration for the degradation of pollutants is important from a practical point of view due to the cost and toxicity, an attempt should also be made to reduce the amount of H_2O_2 required for efficient degradation [26,27].

α-FeOOH as a semiconductor catalyst has been widely used in the degradation of many chlorinated compounds owing to the unique electrical, optical and photoluminescence properties with relatively low band-gap energy (2.2 eV) [28]. The nano-sized α-FeOOH with structures ranging from 1 to 100 nm was proven to have unique physicochemical, surface and optoelectronic properties, as well as improving the visible light photocatalytic activity of the photocatalyst [21]. However, the commercial precipitation technique for α-FeOOH preparation may have several disadvantages related to long time consumption and high temperature, and the precipitation conditions require extremely careful control [29]. Therefore, it is necessary to find a simple and rapid method for the preparation of α-FeOOH. Electrolysis is one of the attractive methods that has been widely used for various applications [30–32] and was explored for a few decades for the synthesis of nano-sized α-FeOOH. However, the use of surplus conventional organic solvents in electrochemical cells urges investigation of other alternative solvents.

In these scenarios, ionic liquids (ILs), which have been widely used as a new kind of reaction media, have abundant charge-carrying ions and are stable in nature, thus making it a potential solvent as well as an electrolyte for the electrolysis of α-FeOOH [33]. Furthermore, ILs can be an alternative to coordinating protective ligands and layers in order to stabilize nano-sized α-FeOOH. This is because nano-sized α-FeOOH is only kinetically stable and will combine to thermodynamically-favored larger metal particles via agglomeration. Although several studies have been conducted to synthesize metal nanoparticles in IL [34,35], the catalyst–ionic liquid interaction and the performance of the catalyst has not been widely investigated.

Therefore, this study reports the synthesis of α-FeOOH by a simple electrochemical method in an ionic liquid, dodecyltrimethylammonium bromide. The crystallinity, morphology, functional characteristics, and surface area of α-FeOOH were studied. The possibility of the synthesized α-FeOOH to serve as a photo-Fenton-like catalyst for 2-chlorophenol (2-CP) degradation under visible light irradiation and its catalysis mechanism was also explored. The kinetics of the photo-Fenton reaction was investigated as well as the reusability and the stability of the catalyst.

2. Experimental

2.1. Materials

2-CP Alfa Aesar®, a German product with 99% purity, was used without further purification. Mono–cationic ionic liquid dodecyltrimethylammonium bromide was purchased from Fisher Scientific (M) Sdn. Bhd., Malaysia. Iron and platinum plates of more than 99.99% purity were obtained from Nilaco, Japan. Sodium oxalate ($Na_2C_2O_4$), isopropanol [$(CH_3)_2CHOH$], and potassium dichromate [$K_2Cr_2O_7$ (Cr(VI))] were purchased from Riedel–deHaën Chemical Co., Germany. KNO_3, NaOH and HCl were obtained from HmbG Chemicals, Malaysia. Deionized water supplied by the Bibby Sterilin Ltd., UK water treatment system was used to prepare all the reagents and pH solutions. Adjustments to the pH were performed using a 0.1 N HCl and 0.1 N NaOH solution.

2.2. Catalyst preparation

The experimental procedures of synthesis of α-FeOOH nanoparticles were similar to those reported in the literature [36–39]. The process was performed in a one-compartment cell equipped with a magnetic stirring bar and a two-electrode configuration. An iron plate (2 cm × 2 cm) anode and a platinum plate (2 cm × 2 cm) cathode were cleaned carefully using 1.0 M HCl followed by deionized water before use. The parallel electrodes with a distance of 2.0 cm were inserted into 15 mL ionic liquid/water solution, with a volume ratio of ionic liquid to water of 1:1. Then electrolysis was conducted at a constant current of 60 mA cm^{-2} and 0 °C under air atmosphere. After electrolysis, the mixture was immersed at 80 °C in an oil bath before being dried overnight at 110 °C to give a brown-colored α-FeOOH powder, which is denoted IL-FeOOH.

For the purpose of comparison, α-FeOOH was also prepared by a post-synthesis method, in which the ionic liquid was introduced to commercial α-FeOOH, and denoted as P-FeOOH. The commercial α-FeOOH was denoted as C-FeOOH.

2.3. Characterization

The crystallinity of IL-FeOOH was confirmed by X-ray diffraction (XRD) recorded on a D8 ADVANCE Bruker X-ray diffractometer using Cu $K\alpha$ radiation at a 2θ angle ranging from 3° to 90°. The phases were identified with the aid of the Joint Committee on Powder Diffraction Standards (JCPDS) files.

The morphology and size of IL-FeOOH were observed using a transmission electron microscope (TEM) (JEOL JEM–2100F). The sample was prepared by drop-casting the IL-FeOOH nanoparticles onto a carbon-coated copper grid in air. The functional groups of IL-FeOOH were identified using a Perkin Elmer Spectrum GX Fourier-transform infrared (FT-IR) Spectrometer using the KBr method with a scan range of 400–4000 cm^{-1}. The surface area of IL-FeOOH was calculated with the Brunnauer–Emmett–Teller (BET) method using a Micromeritics ASAP 2010 instrument.

The zero point charge (pH_{zpc}) of IL-FeOOH was determined using the solid addition method [40]. A series of 100 mL conical flasks, 45 mL of 0.1 M KNO_3 solution was transferred. The pH_0 values of the solution were roughly adjusted from 3 to 11 by adding either 0.1 N HCl or 0.1 N NaOH. The total volume of the solution in each flask was made exactly to 50 mL by adding the KNO_3 solution. The pH_0 of the solutions were then accurately noted. IL-FeOOH (0.15 g) was added to each flask and securely capped, immediately. The suspension was then stirred for 48 h. The pH values of the supernatant liquid were noted. The difference between the initial and final pH (pH_f)

values ($\Delta pH = pH_0 - pH_f$) was plotted against the pH_0. The point of intersection of the resulting curve at which pH_0 gave the pH_{zpc}.

2.4. Catalytic testing

The catalytic activity of the catalyst was tested on a photo-Fenton degradation of 2-CP in a Pyrex batch photoreactor, 140 mm length and 85 mm diameter with a total volume of 0.25 m^3. The catalyst (0.360 g L^{-1}) was added to 200 mL of 2-CP solution at the desired concentration and stirred for 2 h in the dark to achieve adsorption–desorption equilibrium with a stirring rate of 250 rpm. Band gap value of IL-FeOOH (2.75 eV) was determined from plots of the Kubelka–Munk (K–M) function [$f_{K-M} = (h\nu/\lambda)^{1/2}$] as a function of the energy of the excitation light [$h\nu$]. The low band gap value indicates that lower photon energy from visible light irradiation is sufficient to initiate the photoactivity of IL – FeOOH. Moreover, photoluminescence (PL) study indicated that IL – FeOOH exhibits a broad band at 670 nm in the visible region (figure not shown) demonstrating a possible photocatalytic activity of IL – FeOOH in the visible light irradiation system. Therefore, a Philips TL 20 W/52 fluorescent lamp within quartz glass housing (emission spectrum 350–600 nm) with a peak emission at 430 nm was employed as the light source and mounted 10 cm above the solution. The entire set-up was placed inside a chamber covered with aluminum foil to prevent the passage of other lights into the reactor. The initial pH of the solution was 5 and the reaction was carried out at 50 °C. Then the prescribed hydrogen peroxide (H_2O_2) was added and ambient air was bubbled into the system continuously using an air pump (AC 100 – 240 V, 12 W motor) before the reaction was performed for another 3 h under visible light irradiation.

Scavenging study was performed to determine significant reactive species in this study. The scavengers used were sodium oxalate (SO), isopropanol (IP), and potassium dichromate (PD), with same initial concentration of 0.5 mmol L^{-1}. SO was chosen as an effective hole scavenger, and IP as •OH scavenger because it reacts with •OH radicals with a high rate constant of $1.9 \times 109\ M^{-1}\ s^{-1}$ [41]. PD was used as an electron scavenger to determine the presence of photo-generated electron from the catalyst. 0.360 g L^{-1} catalyst with SO, IP or PD was dispersed in 50 mg L^{-1} 2-CP aqueous solution before subjected to visible light irradiation. During the reaction, aliquots of 2 mL were taken out at intervals of 15 min and centrifuged in a Hettich Zentrifugen Micro 120 at 75,000 rpm for 10 min before being analyzed by a double-beam UV–Vis spectrophotometer (Cary 60 UV–Vis Agilent) at 274 nm for the residual concentration of 2-CP.

3. Results and discussion

3.1. Characterization

3.1.1. Crystallinity, phase, structural, and textural studies

The XRD pattern shown in Fig. 1 reveals that diffraction peaks corresponding to (0 2 0), (1 1 0), (1 2 0), (0 2 1), (1 1 1), (1 2 1), (1 4 0), (1 5 1), and (1 6 1) planes match very well with those of bulk α-FeOOH (JCPDS file no. 81-0462), which proves that the nanoparticles collected from the electrolysis cell (IL-FeOOH) are pure orthorhombic phase α-FeOOH without any impurities. The *d*-spacing observed for the strong (1 1 0) facet was 0.418 nm, and this is identical with the facet reported in the literature [42]. This facet is predicted to have a great tendency to be bound with the IL due to its high surface energy [43,44]. The measured BET specific surface area for the nanoparticles was 12.01 $m^2\ g^{-1}$.

3.1.2. Morphological properties

Fig. 2 represents the TEM micrograph of the IL-FeOOH nanocatalyst. Nearly spherical nanoparticles were clearly observed with a diameter range of 5–10 nm (Fig. 2A and B). The size of IL-FeOOH nanoparticles was obviously much smaller than those of synthesized α-FeOOH commonly reported in the literature, which were mostly >20 nm [45,46], signifying the use of IL as a solvent inhibited the growth of the nanoparticles. Further insight into these nanoparticles in higher magnification (Fig. 2B) shows that the IL-FeOOH were partially arrayed, which might be due to average monodispersity of the α-FeOOH nanoparticles [47]. However, the IL-FeOOH nanoparticles in these arrays were still discrete and not fused into larger particles, showing that these nanoparticles have rather high stability upon electrolysis. In addition, the average particle-to-particle distance (d_{pp}) measured was ~2 nm (Fig. 2B), shorter than twice the IL molecule length, which is 3.6 nm [48]. This may be due to the interdigitation of alkyl chains between the two adjacent iron clusters resulting in discrete nanoparticles.

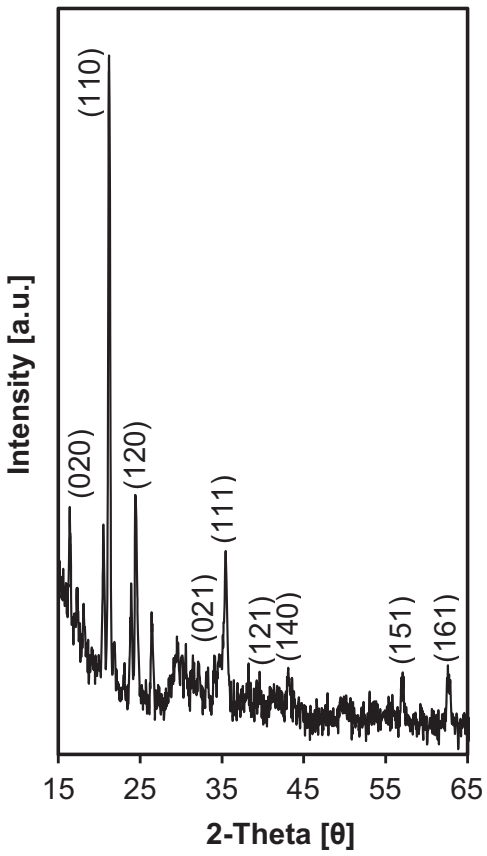

Fig. 1. XRD patterns of IL-FeOOH nanoparticles.

High-resolution transmission electron microscopy (HRTEM) was adopted to further identify the crystallinity of the catalyst. The HRTEM image (Fig. 2C) demonstrates high crystallinity of IL-FeOOH with an ordered crystal lattice, which can be indexed as (1 1 0) plane, whereas the value of the observed interplanar distance (*d*-spacing) agrees with the *d*-spacing value obtained from XRD analysis. The inset image in Fig. 2C demonstrates the fast Fourier transform (FFT) for the lattice image; the bright diffraction spot confirms a single crystal of IL-FeOOH.

3.1.3. Vibrational spectroscopy

In order to verify the bonding between the IL and α-FeOOH surface, IL-FeOOH was further characterized by means of FT-IR spectroscopy. The spectrum was compared with pure IL, post-synthesized commercial α-FeOOH in IL (P-FeOOH), and commercial α-FeOOH (C-FeOOH) spectra. A peak at around 3421 cm^{-1} in the spectra of IL, IL-FeOOH, P-FeOOH, and C-FeOOH, could be attributed to the metal–OH stretching vibrations of the hydroxyl group

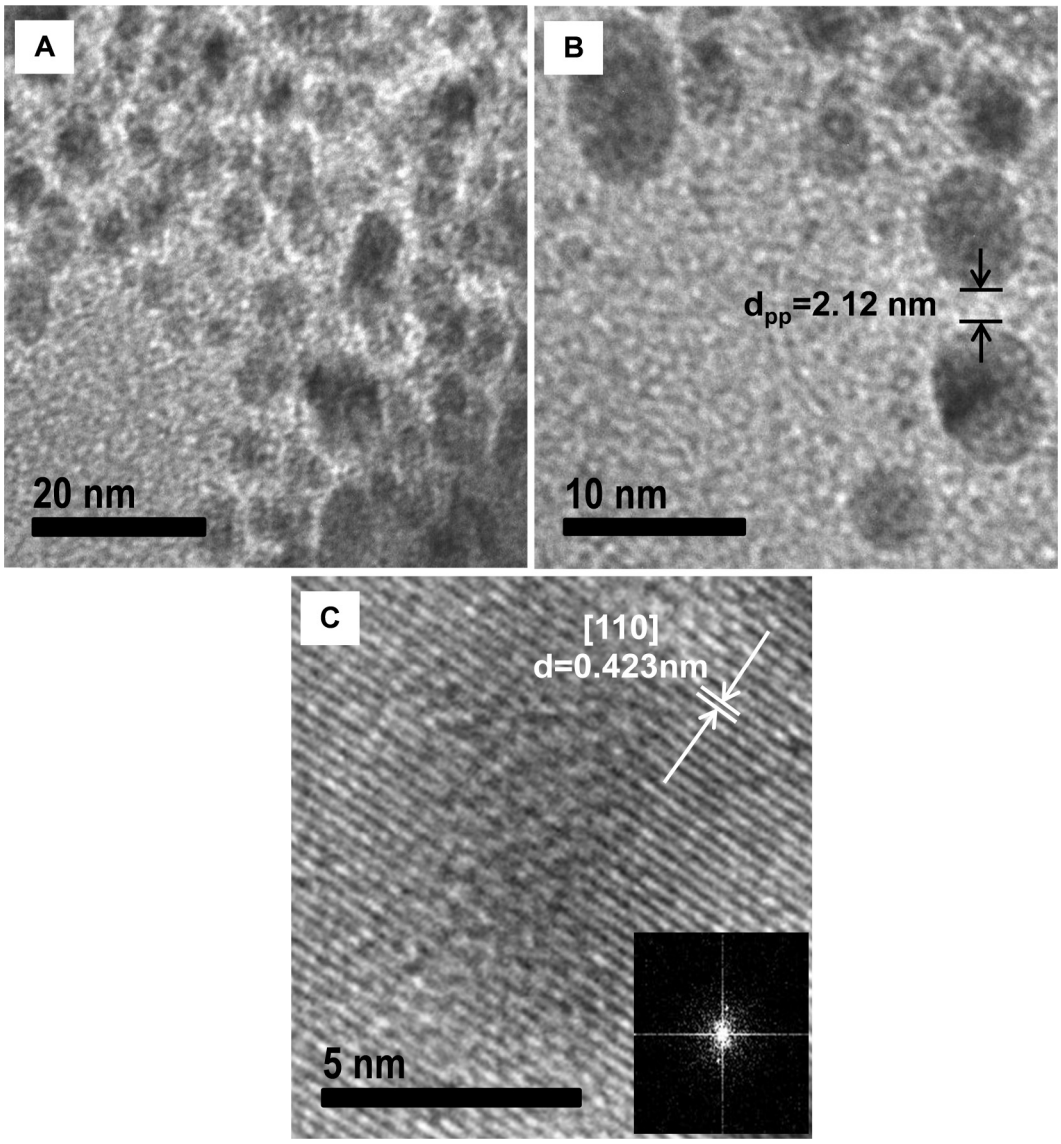

Fig. 2. (A) and (B) TEM image of IL-FeOOH nanoparticles; (C) HRTEM image and the FFT image (as inset).

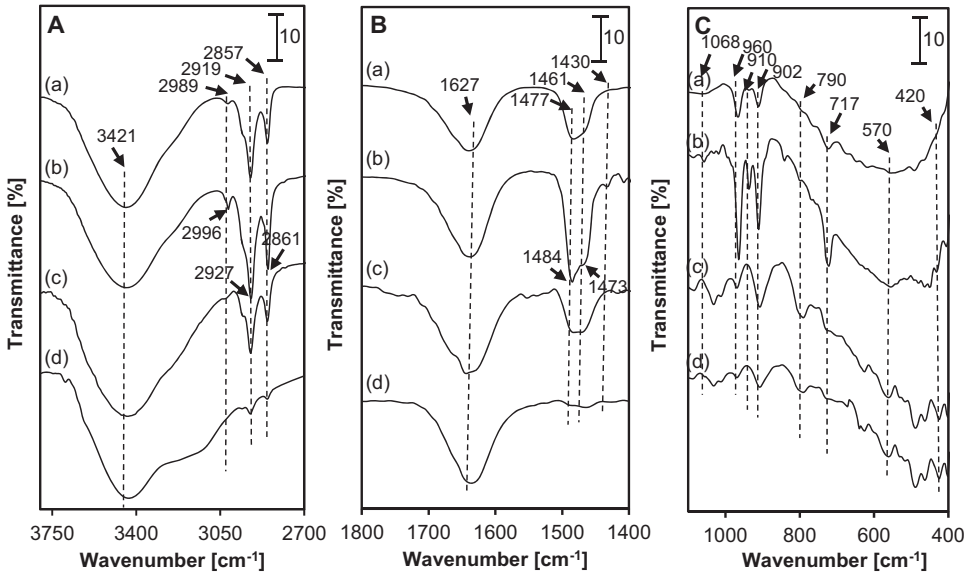

Fig. 3. FT-IR spectra of (a) IL, (b) IL-FeOOH, (c) P-FeOOH, and (d) C-FeOOH. (A) Region 3800–2700 cm^{-1}; (B) region 1800–1400 cm^{-1}; (C) region 1100–400 cm^{-1}.

(Fig. 3A) [35,49]. The peak for IL-FeOOH was smaller than those of P-FeOOH and C-FeOOH, implying that there were less hydroxyl groups adsorbed on the surface of IL-FeOOH compared to the others. Thus, it could be concluded that IL, which acts both as a solvent and electrolyte in the electrolysis process, restricted the adsorption of surface hydroxyl groups. The peak at band 2989 cm^{-1} was attributed to C–H stretching vibrations of the CH_3 terminal group of the methylene chain of IL [47,50]. This peak shifted to 2996 cm^{-1} in the IL-FeOOH, suggesting a higher density of gauche defects in IL-FeOOH rather than in IL. The CH_2 stretching vibrations at band 2919 and 2857 cm^{-1} shown in the IL spectrum were also shifted to higher frequencies (2927 and 2861 cm^{-1}) in the IL-FeOOH, signifying the high density of IL defects or bond strength caused by the tethering of IL on the α-FeOOH surface.

Fig. 3B shows a broad peak centered at band 1627 cm^{-1} in all of the samples, attributed to the bending vibration of the OH group [51]. Doublet peaks observed at band 1477 and 1461 cm^{-1} in the IL spectrum corresponded to the CH_2 scissoring mode of the IL methylene chain. These peaks were shifted to higher frequencies (1484 and 1473 cm^{-1}), and increased in intensity for the IL-FeOOH, apparently due to the increasing number of gauche conformers in the chains [44]. They also shifted to higher frequencies in the P-FeOOH spectrum with similar intensity and broadness with the IL spectrum, suggesting an electrostatic interaction between the IL and α-FeOOH. A new peak was observed in the IL-FeOOH spectrum at band 1430 cm^{-1}, which may correspond to head group vibrations of the IL at the α-FeOOH surface. Other new peaks were also observed at band 1068 and 910 cm^{-1} for IL-FeOOH (Fig. 3C), which can most probably be assigned to a stretching mode of bound C–N^+ from IL to the α-FeOOH surface [44]. Two peaks were clearly observed at 960 and 902 cm^{-1} for all of the samples, particularly sharply emerged in IL-FeOOH spectrum, indicating the C–N^+ stretching band. A clear peak detected at band 790 cm^{-1} in P-FeOOH and C-FeOOH spectra may be attributed to a vibration of Fe^{3+}–OH [52]. According to the literature, this peak illustrates the formation of the OH^- layer around the metal core [33]. The relatively smaller appearance of this peak in the IL-FeOOH spectrum suggests the rigid coordination between the iron core and the headgroup of the IL. A peak at band 717 cm^{-1} in the IL-FeOOH spectrum may be assigned to a free rotation of the IL methylene chain, implying the methylene chain of the IL is pointing outward from the catalyst [44]. Two peaks obviously observed at band 570 and 420 cm^{-1} in P-FeOOH and C-FeOOH corresponded to Fe-O stretching vibration. These peaks were also slighter in the IL-FeOOH spectrum, which may be due to the stabilization effect by IL through the strongly protective ligand that provides electrosteric protection around the iron core [33,53].

For further investigation of the interfacial properties of IL at the α-FeOOH surface, the IL-FeOOH catalyst was evacuated for 1 h prior to IR measurement to remove the physisorbed water, and was subjected to a range of 303–323 K evacuation temperatures. It is observed in Fig. 4A that the intensity of peak at band 3421 cm^{-1} was decreased with increasing temperature, indicating the loss of water from the catalyst surface. The peaks at band 2996, 2927, and 2861 cm^{-1}, which are attributed to the CH_3 terminal group of the methylene chain and the CH_2 stretching vibrations, respectively, show no change in intensity even at 323 K, verifying the robustness of the IL tethering on the α-FeOOH surface. The peak at 1627 cm^{-1} shown in Fig. 4B, which is assigned to the OH group bending vibration, remains unchanged with temperature, further validating the presence of OH^- layer formation around the metal core. The peaks at bands 1469, 1430, and 1068 cm^{-1}, which correspond to the CH_2 scissoring mode of the IL methylene chain, head group vibrations of the IL, and stretching mode of bound C–N^+ from IL to the α-FeOOH surface, respectively, were also unaffected by the elevating temperature, which confirms the stability of the IL-FeOOH. However, the peak at 960 cm^{-1} slowly decreased with increasing temperature, indicating the gradual removal of the unbound surfactant [44].

3.1.4. Proposed reaction pathways for formation of IL-FeOOH

According to the previous studies, the reaction pathway for the formation of IL-FeOOH was proposed as follows (Scheme 1) [36]. Electrolysis of IL solution with a platinum cathode and an iron anode resulted in anodic dissolution of Fe metal to give Fe^{2+} ions (Eq. (1)). At the cathode, two–electron reduction of water molecules occurs to produce hydroxyl ions OH^- (Eq. (2)) [29], which then reacts with Fe^{2+} ion in the system to give iron hydroxide $Fe(OH)_2$ (Eq. (3)). Oxidation of this species produces $Fe(OH)_3$ and subsequent dehydrolysis gives the α-FeOOH (IL-FeOOH) (Eqs. (4) and (5)) [54,55].

$$Fe \rightarrow Fe^{2+} + 2e^- \quad (1)$$

$$2H_2O + 2e^- \rightarrow H_2 + 2OH^- \quad (2)$$

$$Fe^{2+} + 2OH^- \rightarrow Fe(OH)_2 \quad (3)$$

$$4Fe(OH)_2 + 2H_2O + O_2 \rightarrow 4Fe(OH)_3 \quad (4)$$

$$Fe(OH)_3 \rightarrow FeOOH + H_2O \quad (5)$$

Based on the characterization results, it could be proposed that the IL-FeOOH was formed in a reverse micelle structure bound on the α-FeOOH surface (Scheme 1). FTIR analysis confirmed that the headgroups of IL were attached to hydroxyl anion groups around the iron core with a free swinging alkane tail point outward from the catalyst. The interdigitation of alkane chains between two adjacent α-FeOOH units, which was verified by TEM analysis, led to the discrete and high curvature of the nanoparticles surface. Thus, the IL-FeOOH catalyst is very stable and robust, as proved by the evacuated FTIR at elevated temperature.

3.2. Photo-Fenton-like reaction

3.2.1. Performance of the IL-FeOOH photocatalyst

The performance of the IL-FeOOH was examined on the degradation of 2-chlorophenol (2-CP) photo-Fenton-like reaction and compared with the C-FeOOH and P-FeOOH (Fig. 5). It is well–known that α-FeOOH is a practically inactive photocatalyst for the degradation of such organic contaminants in the absence of any oxidizing agent (e.g., H_2O_2) that plays an important role in providing hydroxyl radicals (•OH) for the reaction. However, as can be seen in Fig. 5A, the synthesized IL-FeOOH was able to give 56% of 2-CP degradation under visible light irradiation even in the absence of H_2O_2.This capability is significantly higher than those reported in the literature, which can only degraded less than 10% of 2-CP in the similar reaction system [56]. In fact, the production of •OH can be enhanced drastically by combining the photocatalytic system (UV/metal oxide) with the Fenton-like system (metal oxide/H_2O_2), a so–called photo-Fenton-like system [57]. As shown in Fig. 5A, the 2-CP was successfully degraded up to 85% when using this system. It is presumed that the headgroups of reverse micelle IL that bound at the α-FeOOH surface have trapped the photogenerated electrons at the conduction band (CB) and simultaneously decreased the recombination rate of photo-induced electron–hole pairs at the valence band (VB), which resulted in the enhancement of the 2-CP degradation. However, the absence of reverse micelle structure in P-FeOOH and C-FeOOH catalysts only produced 73% and 63% of the degradation, respectively. The electrostatic interaction between the IL and α-FeOOH of P-FeOOH, which was confirmed by FTIR analysis, could explain the relatively higher degradation percentage of P-FeOOH compared to C-FeOOH. Control experiments under dark

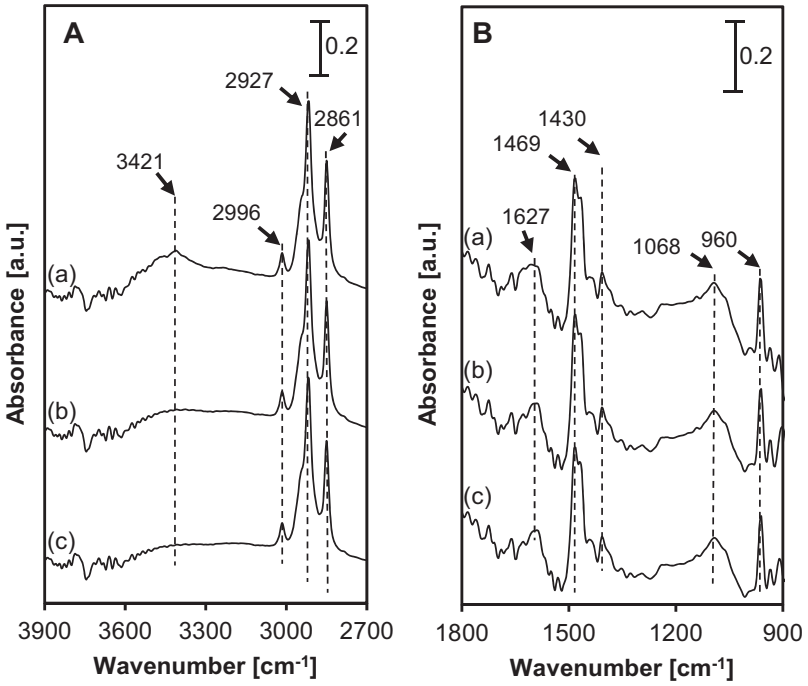

Fig. 4. FT-IR spectra of IL-FeOOH in evacuated system at (a) 303 K, (b) 313 K, and (c) 323 K. (A) Region 3900–2700 cm^{-1}; (B) region 1800–900 cm^{-1}.

conditions were conducted to investigate the importance of visible light irradiation for this system. The result shows that less than 30% of 2-CP degradation was achieved after 8 h of contact time, which indicates the importance of visible light irradiation in this study.

In order to examine the role of IL in the photo-Fenton-like reaction, an excess IL was added to the 2-CP solution containing C-FeOOH, and this system was denoted as IL + FeOOH. As shown in Fig. 5B, the IL + FeOOH showed similar catalytic performance with pure C-FeOOH, in which 65% of maximum degradation percentage of 2-CP has been achieved after 480 min of reaction. From this result, it could be stated that the excess IL in solution has no significant effect on the photo-Fenton-like activity of α-FeOOH. This result supports that the photo-Fenton-like activity enhancement was due to the electrosynthesized IL-FeOOH but not due to the simple electrostatic attraction between $[N]^+$ of IL and negatively charged chlorine $[Cl]^-$ from the 2-CP [58].

3.2.2. Proposed 2-CP degradation mechanism by IL-FeOOH

Next, with the purpose of investigating the degradation mechanism of 2-CP via IL-FeOOH, the effect of scavenging agents was studied and compared with C-FeOOH. Three types of scavengers were used for both systems: potassium dichromate (PD), isopropanol (IP), and sodium oxalate (SO), with the role as a scavenger of photogenerated electrons, hydroxyl radicals (•OH), and photogenerated holes (H^+), respectively [41]. Fig. 6A shows that PD underwent a similar trend of 2-CP degradation with the system using IL-FeOOH, with the highest degradation percentage of 77% after 480 min of the reaction. The degradation efficiency was reduced by half (55%) in the presence of IP, while the addition of SO had significantly decreased the degradation efficiency of 2-CP, confirming the photogenerated hole is the main oxidation species for degrading the 2-CP.

For the case of PD, although the photo-induced electrons at the conduction band have been captured, •OH could still be produced

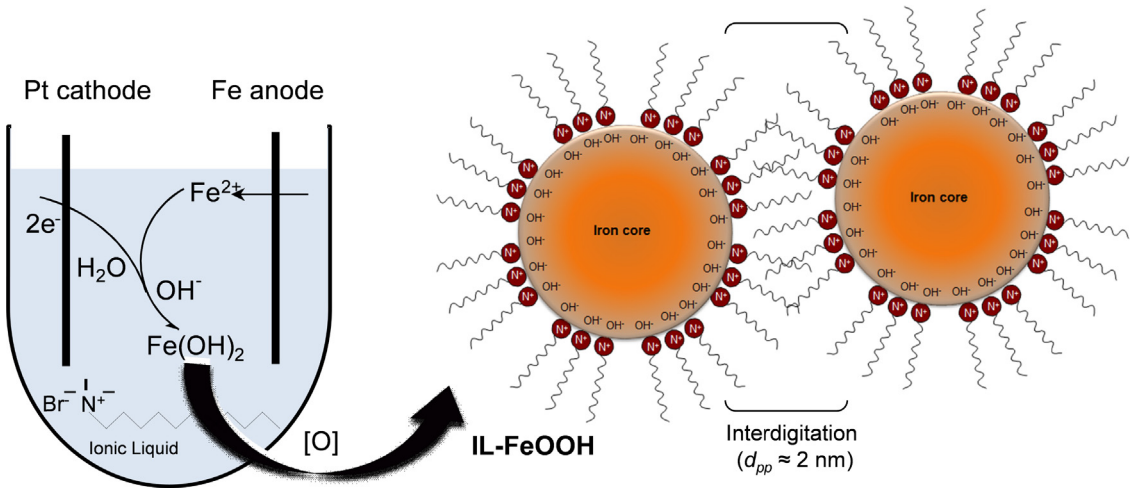

Scheme 1. The proposed reaction pathways for electrosynthesis of IL-FeOOH

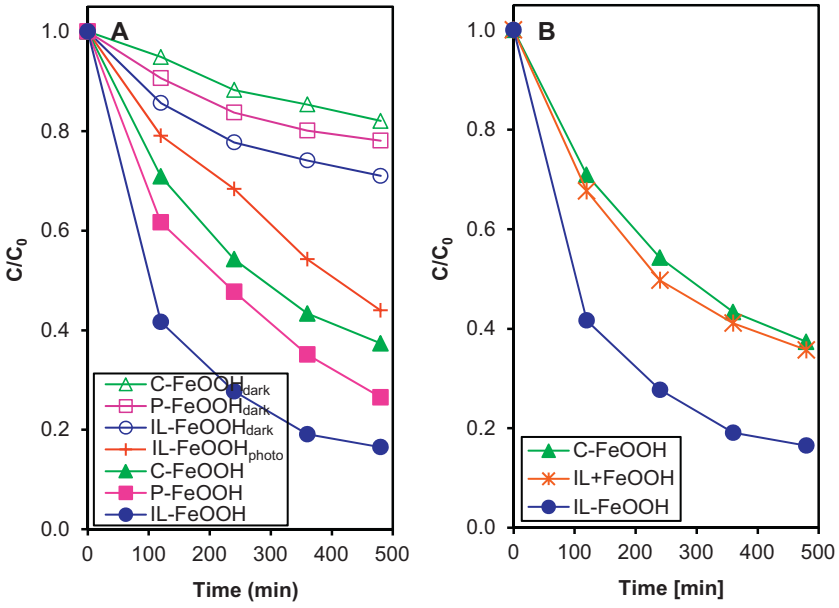

Fig. 5. (A) The performance of catalysts without light irradiation and under light irradiation for photocatalysis of IL-FeOOH, photo-Fenton-like reaction of C-FeOOH, P-FeOOH, and IL-FeOOH catalysts; (B) effects of IL on the photo-Fenton-like activity [pH 5; H_2O_2 concentration 0.156 mM; catalyst dosage 0.30 g L^{-1}; initial concentration 50 mg L^{-1}; temperature 303 K].

via direct photoconversion of H_2O_2 (Eq. (6)) to degrade the 2-CP [59].

$$H_2O_2 \xrightarrow{h\nu} 2^{\bullet}OH \quad (6)$$

In addition, the high oxidation potential of the holes at the valence band (h^+_{VB}) in the IL-FeOOH also permits the direct oxidation of 2-CP to reactive intermediates (Eq. (7)),

$$2\text{-CP} + h^+_{VB} \rightarrow \text{oxidation of 2-CP} \quad (7)$$

The addition of IP to the system shows a rather lower degradation percentage than PD. In fact, •OH could be generated via direct photoconversion of H_2O_2 (Eq. (8)) or photogenerated electron-induced multistep reduction of O_2 (Eqs. (8)–(10)) [35].

$$O_2 + e^- \rightarrow {}^{\bullet}O_2^- \quad (8)$$

$${}^{\bullet}O_2^- + e^- + 2H^+ \rightarrow H_2O_2 \quad (9)$$

$$H_2O_2 + e^- \rightarrow OH^- + {}^{\bullet}OH \quad (10)$$

Thus, trapping the important source •OH in the reaction leaving the direct oxidation shown in Eq. (7) was the only way to degrade the 2-CP.

From the above results, it can be concluded that photogenerated holes play the most important role in the 2-CP degradation via IL-FeOOH catalyst. It was verified that the headgroups of

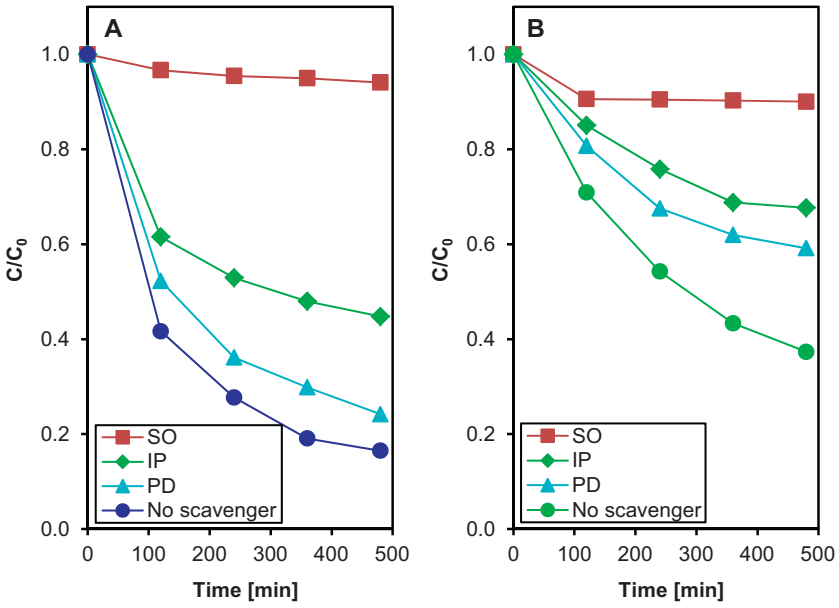

Fig. 6. Photodegradation efficiencies of 2-CP in the presence of hole scavenger, •OH scavenger, and electron scavenger by (A) IL-FeOOH and (B) C-FeOOH [pH 5, H_2O_2 concentration 0.156 mM; catalyst dosage 0.30 g L^{-1}; initial concentration 50 mg L^{-1}; temperature 303 K].

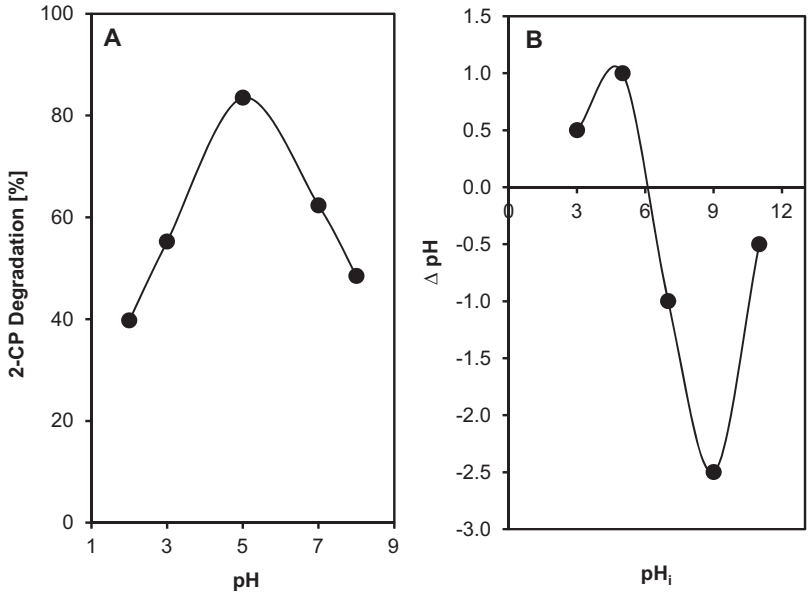

Fig. 7. (A) Effects of pH on the photo-Fenton-like activity of IL-FeOOH; (B) pH of point zero charge (pH_{pzc}) of IL-FeOOH [pH 5, H_2O_2 concentration 0.156 mM; catalyst dosage 0.30 g L^{-1}; initial concentration 50 mg L^{-1}; temperature 303 K].

IL reverse micelle inhibited the recombination of photo-induced electron–hole pairs in the system. Wang and his co-workers also reported a similar phenomenon on visible light photocatalysis using bismuth oxyiodide (BiOI) modified by IL solution [35].

Fig. 6B shows that a similar trend was also observed when using the C-FeOOH, but with a comparatively lower degradation percentage of 2-CP in all cases of scavengers studied. The absence of IL in the system might be the main reason for the lower effectiveness of the C-FeOOH. It could be seen that the photogenerated holes also play an important role in this study, followed by •OH and photogenerated electrons. The proposed electron trapping occurrences for both catalysts are illustrated in Scheme 2.

3.2.3. Effect of pH

The influence of initial pH solution on the degradation of 2-CP was studied in the range of 3.0–7.0 and the result is shown in Fig. 7A. pH 5 was found to be the optimum pH, which gave 85% of the degradation percentage of 2-CP. This result could be explained by the zero point charge (pH_{zpc}) basis of IL-FeOOH, which was determined to be six (Fig. 7B). At pHs higher than the pH_{zpc}, the surface of the IL-FeOOH became negatively charged and this did not favor the interaction with 2-CP [60]. Moreover, the H_2O_2 also tends to decompose and the oxidation potential of the •OH decreases with increasing pH [61]. In contrast, at pHs lower than pH_{zpc}, the higher electronegativity chlorine anions of 2-CP are electrostatically attracted to the positively charged IL-FeOOH surface, which eventually enhanced the degradation. The optimum reaction conditions at pH 5 are in parallel with the industrial phenolic wastewater, which is almost in neutral condition. Therefore, the first adjustment pH process could be alleviated and this will be a benefit from the economical point of view.

3.2.4. Effect of H_2O_2 concentration

H_2O_2 plays a significant role as an oxidizing agent in the photo-Fenton-like reaction. Thus, the selection of an optimal H_2O_2 concentration for the maximum degradation of 2-CP is important from a practical approach to the cost and toxicity [27]. Herein, the initial concentration of H_2O_2 was examined in the range of 0.1 to 0.5 mM and the results are shown in Fig. 8. It could be observed that the degradation of 2-CP was increased by increasing the initial concentration, and maximum degradation was achieved when using 0.15 mM H_2O_2. This is apparently due to the improved oxidation power since H_2O_2 may split photolytically to generate hydroxyl radicals directly. However, further increases in H_2O_2 concentration resulted in a decrease of the 2-CP degradation. This may be on account of the higher concentration of H_2O_2 producing an excess amount of reactive •OH radicals, which subsequently tend to generate less reactive OOH radical [62]. Remarkably, the

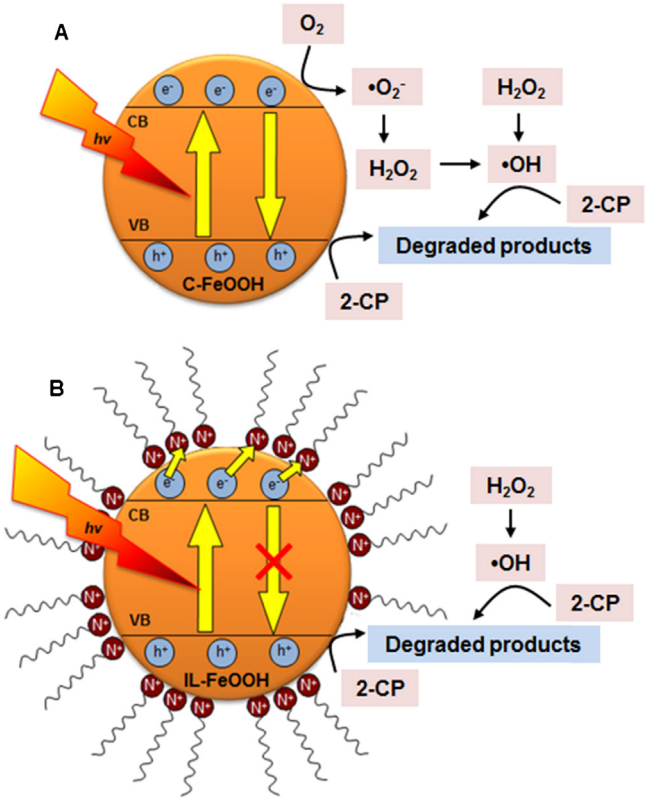

Scheme 2. Schematic illustration of 2-CP photodegradation over (A) C-FeOOH, and (B) photogenerated electron trapping by IL headgroups of IL-FeOOH

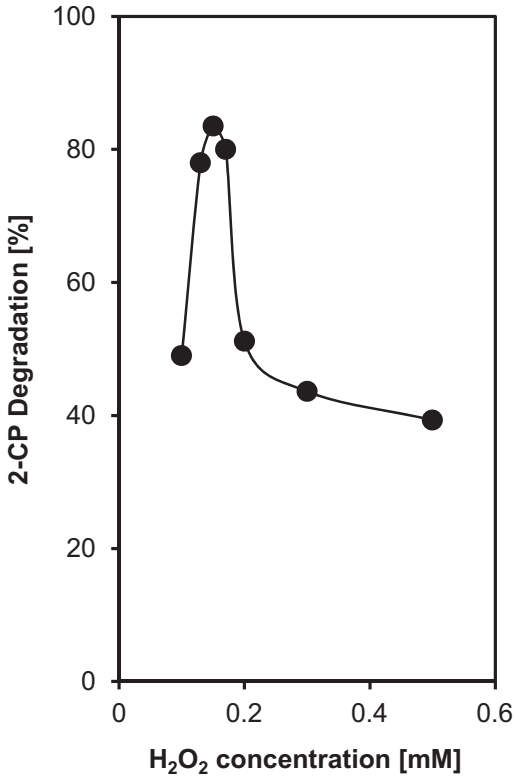

Fig. 8. Effects of H_2O_2 concentration on the photo-Fenton-like activity of IL-FeOOH [pH 5; catalyst dosage 0.30 g L^{-1}; initial concentration 50 mg L^{-1}; temperature 303 K].

consumed optimum amount of H_2O_2 for 2-CP degradation using IL-FeOOH was far less than such reactions reported in the literature [14,21–25], which almost required 2–20 mM H_2O_2. The disproportionate excess concentration of the H_2O_2 may be induced by the high electron–hole recombination rate. Therefore, the inhibition of electron–hole recombination by the reverse micelle IL lessen the need for generating •OH radicals in this efficient photo-Fenton-like reaction.

3.2.5. Effect of temperature

The effect of temperature on the photodegradation of 2-CP using IL-FeOOH was studied in the range of 303–323 K and the result is shown in Fig. 9. A significant enhancement was observed from 85% to quantitative degradation when the temperature was increased from 303 to 323 K. The illumination time could also be decreased by half to completely degrade the 2-CP at 323 K in comparison with the only 85% degradation achieved at 303 K after 480 min. This may be due to the increasing temperature also increasing the reaction rate between the H_2O_2 and the IL-FeOOH catalyst, thus accelerating the rate of generation of the oxidizing species [27]. Similar results were also reported in the literature using synthesized α-FeOOH with different particle sizes [21,25].

Although the operation temperature for IL-FeOOH was relatively higher compared to the other α-FeOOH, it only required a small amount of H_2O_2 (0.156 mM) and catalyst dosage (0.03 g L^{-1}), as well as nearly neutral pH conditions (pH 5) for almost complete degradation of a standard concentration of 2-CP (50 mg L^{-1}) [14,21,22,24,25]. Compared to other studies which most commonly required more than ten times greater H_2O_2 amount (>2 mM), catalyst dosage greater than 0.20 g L^{-1} and highly acidic conditions IL-FeOOH had a remarkable ability to degrade the 2-CP. Thus, apart from the nanosize of the IL-FeOOH, it is noteworthy that the reverse micelle formation around the IL-FeOOH greatly

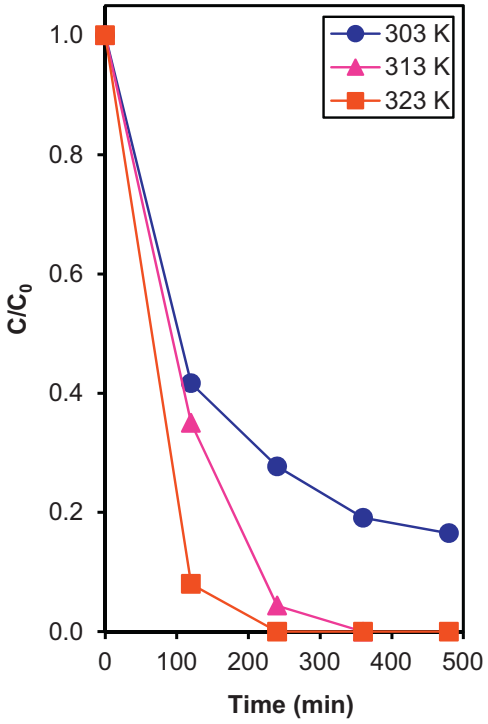

Fig. 9. Effects of temperature on the photo-Fenton-like activity of IL-FeOOH [pH 5; H_2O_2 concentration 0.156 mM, catalyst dosage 0.30 g L^{-1}; initial concentration 50 mg L^{-1}].

inhibited the recombination of electron–hole pairs, which leads to the plausible mild operating conditions.

3.3. Reusability of the catalyst

Reusability is an important issue to be considered when dealing with photocatalyst [63]. Repeated experiments were carried out using IL-FeOOH in order to study the reusability of the catalyst for the degradation of 2-CP (Fig. 10). It can be observed that after three repeated cycles, the catalyst was still active with just a small decrease in 2-CP degradation percentage from 98% to 88%. However, a relatively significant decrease of degradation was observed after the fourth cycle (85%). The results suggest that the reverse

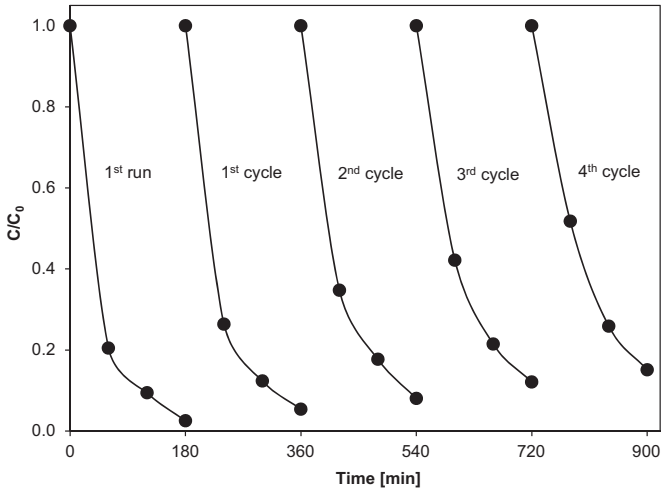

Fig. 10. Stability of IL-FeOOH catalyst after subsequent reactions [pH 5; H_2O_2 concentration 0.156 mM, catalyst dosage 0.30 g L^{-1}; initial concentration 50 mg L^{-1}, temperature is 323 K].

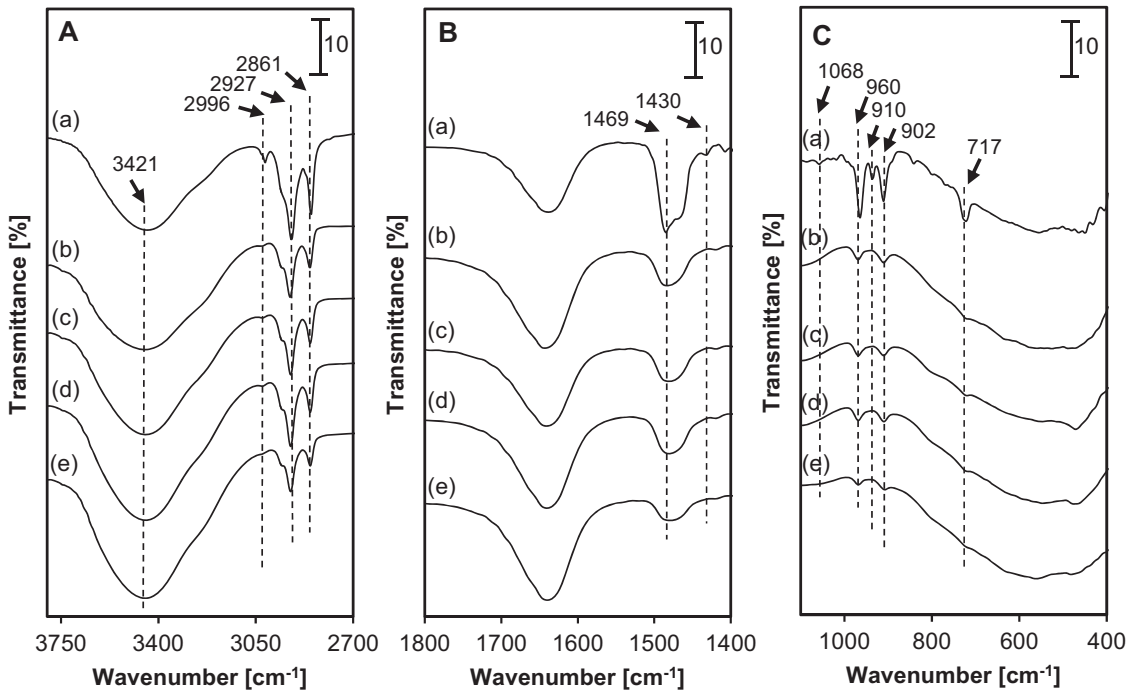

Fig. 11. FT-IR spectra of IL-FeOOH (a) before photo-Fenton-like reaction, and after subsequent reactions (b) 1st run, (c) 2nd run, (d) 3rd run, and (d) 4th run. (A) Region 3800–2700 cm^{-1}; (B) region 1800–1400 cm^{-1}; (C) region 1100–400 cm^{-1}.

micelle bound on the catalyst most probably gradually detached from the catalyst surface after three cycles and induced the catalyst aggregation, which therefore reduced the 2-CP degradation efficiency.

In order to further investigate the structure of the IL-FeOOH after repeated photo-Fenton-like reactions, FT-IR analysis was performed after every cycle. As shown in Fig. 11A, the peak at 3421 cm^{-1}, which was attributed to the stretching vibrations of hydroxyl groups, increased in intensity along the repeated experiments, implying more hydroxyl groups from 2-CP were adsorbed on the surface of IL-FeOOH. The peak at 2996 cm^{-1} is attributed to the CH_3 terminal group of the methylene chain. The disappearance of this peak after three cycles verified that the detachment of the IL alkane chain from the catalyst surface, and suggests the possibility of the catalyst aggregation. The CH_2 stretching vibrations at 2927 and 2861 cm^{-1}, which indicates the tethering of IL on the α-FeOOH surface, were clearly observed even after three cycles, suggesting the presence of IL around the catalyst surface [47]. Fig. 11B shows the peak at 1469 cm^{-1}, which is attributed to the CH_2 scissoring mode of IL methylene chain, decreased in intensity with increased cycles indicating that the electrostatic interaction between the IL and the catalyst became weaker. The peak at 1430 cm^{-1} was shifted to lower frequencies and then disappeared after the third cycle, demonstrating that the head group of IL was removed from the catalyst surface. The absence of the 1068 cm^{-1} peak after first run indicates the disappearance of bound C–N^+ from IL to the α-FeOOH

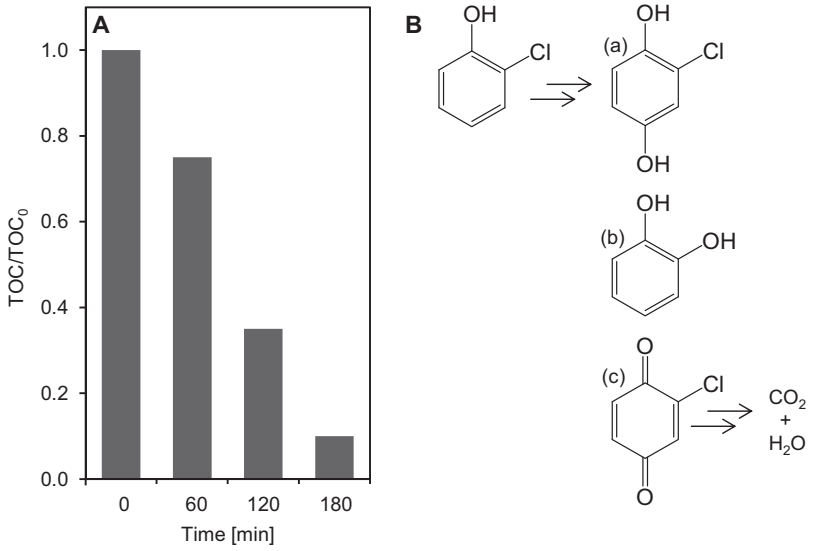

Fig. 12. (A) TOC reduction levels after 3 h of reaction time; (B) simplified mechanism for the photo-Fenton-like degradation of 2-CP [pH 5, H_2O_2 concentration 0.156 mM; catalyst dosage 0.30 g L^{-1}; initial concentration 50 mg L^{-1}; temperature 323 K].

surface, leaving only the electrostatic interactions between the IL head groups and the catalyst surface (Fig. 11C). This is in line with the peaks at 960, 910, and 902 cm^{-1} after three cycles, which is attributed to the C–N^+ stretching band. The peak at 717 cm^{-1}, which corresponds to the free rotation of the IL methylene chain, also disappeared after the third cycle, suggesting the removal of the pointed outward methylene chain of IL from the catalyst. These results suggest that the reverse micelle structures bound on the IL-FeOOH surface are detached from the catalyst surface. After three subsequent cycles, the headgroups of IL are weakly attached to the catalyst surface and no alkane tails are pointing outward. This phenomenon might induce the aggregation of the catalyst and result in the stability decrease of IL-FeOOH, which is in accordance with the stability test result.

3.4. Total organic carbon (TOC) evaluation

Fig. 12 shows the TOC level of 2-CP solution with IL-FeOOH catalyst. The result indicates that the TOC level decreased to 10% after 3 h of irradiation time. This high mineralization rate indicates the efficient decay of 2-CP to simpler compounds. According to the literature [64], the decay of 2-CP involved several steps before total removal of all organic intermediates was achieved. Since direct hole oxidation was the main reacting process in this system, direct electron transfer from 2-CP to IL-FeOOH gives a positive radical which can be converted into a chlorodihydroxycyclohexadienyl radical (ClDHCHDR) after nucleophilic water addition, or into chlorophenoxyl radical (CPR) after deprotonation. For ClDHCHDR, •OH addition in the para position to 2-CP followed by H-abstraction leads to 2-chlorohydroquinone (a), while addition in ortho position followed by Cl-abstraction gives catechol (b). Meanwhile, for CPR, the presence of dissolved O_2 may lead to the formation of chlorobenzoquinone (c). Further oxidation of the aromatic intermediates (a–c) leads to ring opening and may induce the formation of carboxylic acids, later to the total mineralization of 2-CP to H_2O and CO_2.

4. Conclusion

The results reveal the feasibility to synthesize well-dispersed α-FeOOH nanoparticles in a diameter range of 5–10 nm via a facile electrosynthesis in ionic liquid. Ionic liquid was successfully demonstrated to play a dual role as electrolyte and solvent. Reverse micelle formation bound on the IL-FeOOH surface was found to stabilize and miniaturize the nanoparticles. The IL-FeOOH were verified to positively serve as a photo-Fenton-like catalyst for complete degradation of 2-chlorophenol under mild operating conditions, which induced the inhibition of the photo-induced electron–hole pairs recombination where the photogenerated electron could be trapped by the reverse micelle bound on the catalyst surface. Nearly neutral conditions of pH 5 were able to completely degrade 2-CP within 180 min with a small amount of H_2O_2 (0.156 mM). After four subsequent reactions, the IR study revealed that the catalyst was still stable. Significantly, this α-FeOOH synthesis method could be a great advantage in the future development of nanotechnology.

Acknowledgement

The authors are grateful for the financial support of the Research University Grant from Universiti Teknologi Malaysia (Grant No. 01H59 and 4L112), the Exploration Research Grant Scheme from Ministry of Higher Education Malaysia, the awards of the King's Scholarship and Fellowship Scheme from Universiti Malaysia Pahang (Rohayu Jusoh), and also the support of the Hitachi Scholarship Foundation.

References

[1] N.C. Tolosa, M.-C. Lu, H.D. Mendoza, A.P. Rollon, Appl. Catal., A 401 (2011) 233–238.
[2] S. Mozia, K. Bubacz, M. Janus, A.W. Morawski, J. Hazard. Mater. 128 (2012) 203–204.
[3] A.A. Jalil, S. Triwahyono, N.A.M. Razali, N.H.H. Hairom, A. Idris, M.N.M. Muhid, A. Ismail, N.M.N. Yahaya, N.A.L. Ahmad, H. Dzinun, J. Hazard. Mater. 174 (2010) 581–585.
[4] A.A. Jalil, N.F.A. Panjang, S. Akhbar, M. Sundang, N. Tajuddin, S. Triwahyono, J. Hazard. Mater. 148 (2007) 1–5.
[5] W. Viessman Jr., M.J. Hammer, Water Supply and Pollution Control, Pearson Education, Seventh ed., Upper Saddle River, NJ, USA, 2005.
[6] R. Gonzalez–Olmos, F. Holzer, F.-D. Kopinke, A. Georgi, Appl. Catal., A 398 (2011) 44–53.
[7] A.N. Soon, B.H. Hameed, Appl. Catal., A 450 (2013) 96–105.
[8] H.-E. Kim, J. Lee, H. Lee, C. Lee, Appl. Catal., B 115 (2012) 219–224.
[9] M. Munoz, Z.M. de Pedro, J.A. Casas, J.J. Rodriguez, J. Hazard. Mater. 190 (2011) 993–1000.
[10] D.H. Metz, M. Meyer, A. Dotson, E. Beerendonk, D.D. Dionysiou, Water Res. 45 (2011) 3969–3980.
[11] K.C. Christoforidis, M. Louloudi, E.R. Milaeva, Y. Deligiannakis, J. Catal. 290 (2010) 153–162.
[12] X. Xu, X. Shen, H. Zhou, D. Qiu, G. Zhu, K. Chen, Appl. Catal., A 455 (2013) 183–192.
[13] D. Zhao, G. Sheng, C. Chen, X. Wang, Appl. Catal., B 111 (2012) 303–308.
[14] G.B. Ortiz de la Plata, O.M. Alfano, A.E. Cassano, Appl. Catal., B 95 (2010) 1–13.
[15] D.J. Kalota, D.C. Silverman, Corrosion 50 (1994) 138–145.
[16] A. Burbano, D. Dionysiou, M. Suidam, T. Richardson, Water Sci. Technol. 47 (2003) 165–171.
[17] B.P. Nenavathu, A.V.R.K. Rao, A. Goyal, A. Kapoor, R.K. Dutta, Appl. Catal., A 459 (2013) 106–113.
[18] L. Ge, C. Han, J. Liu, Y. Li, Appl. Catal., A 409–410 (2011) 215–222.
[19] X. Zhang, Y. Tang, Y. Li, Y. Wang, X. Liu, C. Liu, S. Luo, Appl. Catal., A 457 (2013) 78–84.
[20] L. Shi, X. Wang, N. Li, C. Huai, J. Liu, ISRN Anal. Chem. (2012) 951465.
[21] G.B. Ortiz de la Plata, O.M. Alfano, A.E. Cassano, Water Sci. Technol. 258 (2010) 3019–3116.
[22] G.B. Ortiz de la Plata, O.M. Alfano, A.E. Cassano, Chem. Eng. J. 137 (2008) 396–410.
[23] M.-C. Lu, J.-N. Chen, H.-H. Huang, Chemosphere 46 (2002) 131–136.
[24] M.-C. Lu, Chemosphere 40 (2000) 125–130.
[25] T.R. Gordon, A.L. Marsh, Catal. Lett. 132 (2009) 349–354.
[26] E.-K. Kim, S.-J. Lee, S.-H. Moon, B.-T. Jeon, C.-B. Ahn, B. Kim, B.-O. Lim, P.-J. Park, Food Chem. 117 (2009) 232–240.
[27] J.-H. Sun, S.-P. Sun, G.-L. Wang, L.-P. Qiao, Dyes Pigm. 74 (2007) 647–652.
[28] A. Gajović, A.M.T. Silva, R.A. Segundo, S. Šturm, B. Jančar, M. Čeh, Appl. Catal., B 103 (2011) 351–361.
[29] C.K. Gupta, Chemical Metallurgy: Principles and Practice, Wiley-VCH Verlag GmbH&Co., Weinheim, Germany, 2003.
[30] H. Kim, S.H. Moon, Carbon 49 (2011) 1491–1501.
[31] H.T. Kim, J.S. Yoo, H.-I. Joh, H. Kim, S.H. Moon, Int. J. Hydrogen Energy 36 (2011) 1606–1612.
[32] H.T. Kim, H.-I. Joh, S.H. Moon, J. Power Sources 195 (2010) 1352–1358.
[33] C. Vollmer, C. Janiak, Coord. Chem. Rev. 255 (2011) 2039–2057.
[34] N. Liu, D. Wu, H. Wu, F. Luo, J. Chen, Solid State Sci. 10 (2008) 1049–1055.
[35] Y. Wang, K. Deng, L. Zhang, J. Phys. Chem. C 115 (2011) 14300–14308.
[36] A.A. Jalil, N. Kurono, M. Tokuda, Synlett 12 (2001) 1944–1946.
[37] A.A. Jalil, N. Kurono, M. Tokuda, Synthesis 18 (2002) 2681–2686.
[38] N.F. Jaafar, A.A. Jalil, S. Triwahyono, M.N.M. Muhid, N. Sapawe, M.A.H. Satar, H. Asaari, Chem. Eng. J. 191 (2012) 112–122.
[39] N. Sapawe, A.A. Jalil, S. Triwahyono, S.H. Adam, N.F. Jaafar, M.A.H. Satar, Appl. Catal., B 125 (2012) 311–323.
[40] N.A. Oladoja, Y.D. Aliu, J. Hazard. Mater. 164 (2009) 1496–1502.
[41] W. Wang, Y. Yu, T. An, G. Li, H.Y. Yip, J.C. Yu, P.K. Wong, Environ. Sci. Technol. 46 (2012) 4599–4606.
[42] R.M. Cornell, U. Schwertmann, The Iron Oxides: Structure, Properties, Reactions, Occurrences, and Uses, second ed., Wiley-VCH Verlag GmbH&Co., Weinheim, Germany, 2003.
[43] N. Zhao, W. Ma, Z. Cui, W. Song, C. Xu, M. Gao, ACS Nano 3 (2009) 1775–1780.
[44] B. Nikoobakht, M.A. El-Sayed, Langmuir 17 (2001) 6368–6374.
[45] V. Rădiţoiu, L. Diamandescu, M.C. Corobea, A. Rădiţoiu, N. Popescu-Pogrion, C.A. Nicolae, J. Cryst. Growth 348 (2012) 40–46.
[46] L. Song, S. Zhang, Colloids Surf., A (2009) 217–220.
[47] W. Cheng, S. Dong, E. Wang, Langmuir 19 (2003) 9434–9439.
[48] Z.E. Proverbio, P.V. Messina, J. Ruso, G. Prieto, P.C. Schulz, F. Sarmiento, J. Argent. Chem. Soc. 94 (2006) 19–30.
[49] M.A.Z. Abidin, A.A. Jalil, S. Triwahyono, S.H. Adam, N.H.N. Kamarudin, Biochem. Eng. J. 35 (2004) 967–974.
[50] S.M. Sidik, A.A. Jalil, S. Triwahyono, S.H. Adam, M.A.H. Satar, B.H. Hameed, Chem. Eng. J. 203 (2012) 9–18.

[51] M. Ristić, S. Musić, M. Godec, J. Alloys Compd. 417 (2006) 292–299.
[52] J.L. Bishop, E. Murad, J. Raman Spectrosc. 35 (2004) 480–486.
[53] Y. Nie, C. Hu, J. Qu, X. Zhao, Appl. Catal., B 87 (2009) 30–36.
[54] P. Hu, D. Pan, S. Zhang, J. Tian, A.A. Volinsky, J. Alloys Compd. 509 (2011) 3991–3994.
[55] S. Krehula, S. Popović, S. Musić, Mater. Lett. 54 (2002) 108–113.
[56] J. Bandara, J.A. Mielczarski, A. Lopez, J. Kiwi, Appl. Catal., B 34 (2001) 321–333.
[57] M. Klavarioti, D. Mantzavinos, D. Kassinos, Environ. Int. 35 (2009) 402–417.
[58] B. Jain, A. Uppal, P.K. Gupta, K. Das, J. Mol. Struct. 1032 (2013) 23–28.
[59] H. deLasa, B. Serrano, M. Salaices, Photocatalytic Reaction Engineering, Springer, New York, 2005.
[60] N. Sapawe, A.A. Jalil, S. Triwahyono, R.N.R.A. Sah, N.W.C. Jusoh, N.H.H. Hairom, J. Effendi, Appl. Catal., A 456 (2013) 144–158.
[61] H.R. Eisenhauer, J. Water Pollut. Control Fed. 36 (1964) 1117–1127.
[62] N. Kang, D.S. Lee, J. Yoon, Chemosphere 47 (2002) 915–924.
[63] A. Idris, E. Misran, N. Hassan, A.A. Jalil, C.E. Seng, J. Hazard. Mater. 227–228 (2012) 309–316.
[64] I. Ilisz, A. Dombi, K. Mogyorósi, A. Farkas, I. Dékány, Appl. Catal., B 39 (2002) 247–256.